1521-009X/49/6/459–469$35.00
DRUG METABOLISM AND DISPOSITION

https://doi.org/10.1124/dmd.120.000325
Drug Metab Dispos 49:459–469, June 2021

Reversible and Irreversible Inhibition of Cytochrome P450 Enzymes by Methylophiopogonanone A[S]

Dong-Zhu Tu,[1] Xu Mao,[1] Feng Zhang, Rong-Jing He, Jing-Jing Wu, Yue Wu, Xiao-Hua Zhao, Jiang Zheng, and Guang-Bo Ge

Institute of Interdisciplinary Integrative Medicine Research, Shanghai University of Traditional Chinese Medicine, Shanghai, China (D.-Z.T., F.Z., R.-J.H., Y.W., X.-H.Z., G.-B.G.); Heilongjiang Key Laboratory of Tissue Damage and Repair, Mudanjiang Medical University, Heilongjiang, China (X.M.); Wuya College of Innovation, Shenyang Pharmaceutical University, Shenyang, China (X.M., J.Z.); Department of Clinical Pharmacology, College of Pharmacy, Dalian Medical University, Dalian, China (J.-J.W.); and State Key Laboratory of Functions and Applications of Medicinal Plants, Key Laboratory of Pharmaceutics of Guizhou Province, Guizhou Medical University, Guiyang, Guizhou, China (J.Z.)

Received December 4, 2020; accepted March 9, 2021

ABSTRACT

Methylophiopogonanone A (MOA), an abundant homoisoflavonoid bearing a methylenedioxyphenyl moiety, is one of the major constituents in the Chinese herb *Ophiopogon japonicas*. This work aims to assess the inhibitory potentials of MOA against cytochrome P450 enzymes and to decipher the molecular mechanisms for P450 inhibition by MOA. The results showed that MOA concentration-dependently inhibited CYP1A, 2C8, 2C9, 2C19, and 3A in human liver microsomes (HLMs) in a reversible way, with IC_{50} values varying from 1.06 to 3.43 μM. By contrast, MOA time-, concentration-, and NADPH-dependently inhibited CYP2D6 and CYP2E1, along with K_I and k_{inact} values of 207 μM and 0.07 minute^{-1} for CYP2D6, as well as 20.9 μM and 0.03 minutes^{-1} for CYP2E1. Further investigations demonstrated that a quinone metabolite of MOA could be trapped by glutathione in an HLM incubation system, and CYP2D6, 1A2, and 2E1 were the major contributors to catalyze the metabolic activation of MOA to the corresponding *O*-quinone intermediate. Additionally, the potential risks of herb-drug interactions triggered by MOA or MOA-related products were also predicted. Collectively, our findings verify that MOA is a reversible inhibitor of CYP1A, 2C8, 2C9, 2C19, and 3A but acts as an inactivator of CYP2D6 and CYP2E1.

SIGNIFICANCE STATEMENT

Methylophiopogonanone A (MOA), an abundant homoisoflavonoid isolated from the Chinese herb *Ophiopogon japonicas*, is a reversible inhibitor of CYP1A, 2C8, 2C9, 2C19, and 3A but acts as an inactivator of CYP2D6 and CYP2E1. Further investigations demonstrated that a quinone metabolite of MOA could be trapped by glutathione in a human liver microsome incubation system, and CYP2D6, 1A2, and 2E1 were the major contributors to catalyze the metabolic activation of MOA to the corresponding *O*-quinone intermediate.

Introduction

Ophiopogonis radix (also named mai-dong in Chinese) is a commonly used edible herb in East Asia. Currently, dozens of mai-dong prepared herbal products or health foods (such as sheng-mai-yin decoction, shen-mai injection, and mai-dong soup) have been marketed for preventing and treating a variety of disorders, including cardiovascular disease and various types of cancer (Chen et al., 2016a). In clinical settings, to treat the diseases in a more efficient way, mai-dong prepared herbal products have been widely used in combination with a wide range of Western drugs, in which most therapeutic drugs are the substrates of human cytochrome P450 enzymes (P450s). It has been reported that some mai-dong prepared herbal products (such as shen-mai injection and dengzhan shengmai capsule) can inhibit a panel of hepatic P450s in liver microsomes from both rat and human (Xia et al., 2010; Chen et al., 2016b). However, the key constituents in mai-dong responsible for P450 inhibition and the related inhibitory mechanism(s) still remain unknown.

Bygone investigations have discovered that the Chinese herb mai-dong contains several classes of ingredients, including homoisoflavonoids, steroidal saponins, and polysaccharides (Chen et al., 2016a; Zhao et al., 2017; Fang et al., 2018; Chen et al., 2019; Tan et al., 2019; Tian

This study was financially supported by the National Natural Science Foundation of China [81773810, 81922070, 81973286, 81773687], the National Key Research and Development Program of China [2020YFC0845400, 2017YFC1700200], Program of Shanghai Academic/Technology Research Leader [18XD1403600], Shanghai Talent Development Fund [2019093], Shuguang Program [18SG40], and the Shanghai Education Development Foundation and Shanghai Municipal Education Commission, the Key R&D and Transformation Science and Technology Cooperation Project of Qinghai Province [2019-HZ-819] and Program for Innovative Leading Talents of Qinghai Province [2018 and 2019].

The authors declare no competing interests.

[1]D.-Z.T. and X.M. contributed equally to this work.

https://dx.doi.org/10.1124/dmd.120.000325.

[S] This article has supplemental material available at dmd.aspetjournals.org.

ABBREVIATIONS: AUC, area under the plasma concentration-time curve; CAT, catalase; G-6-P, D-glucose-6-phosphate; G-6-PDH, glucose-6-phosphate dehydrogenase; GSH, glutathione; HDI, herb-drug interaction; HLM, human liver microsome; HP LC, High performance liquid chromatography; IS, internal standard; LC-MS, liquid chromatograph-mass spectrometer; *m/z*, mass-to-charge ratio; MDP, methylenedioxyphenyl; MOA, methylophiopogonanone A; P450, cytochrome P450 enzyme; PDB, protein data bank; PBS, potassium phosphate buffer; SOD, superoxide dismutase; t_R, retention time.

et al., 2019; Zhan et al., 2019). Among all reported ingredients, the homoisoflavonoids (such as methylophiopogonanone A and its analogs) have been identified as the principal bioactive compounds and marker compounds of mai-dong, which have been found to have broad biologic activities, including anticancer, anti-inflammatory, and antibacterial activities (Zhu et al., 2004; Lin et al., 2010; Li et al., 2012; Wang et al., 2017, 2019). As one of the most abundant homoisoflavonoid constituents occurring in *Ophiopogon japonicas* (up to 0.19 mg/g dried materials), methylophiopogonanone A (MOA) has drawn increasing attention from both phytochemists and pharmacologists (Ma et al., 2009; Wang et al., 2013; He et al., 2016) owing to its diverse pharmacological functions, such as anticancer, anti-inflammatory, and antibacterial effects (Li et al., 2012; Liang et al., 2012; He et al., 2016). Notably, MOA is a representative compound of the naturally occurring homoisoflavonoids, and all of these compounds bear a methylenedioxyphenyl (MDP) moiety at the C4′-C5′ sites (Fig. 1). It is well known that the MDP moiety can be bioactivated by mammalian cytochrome P450 enzymes. Such biotransformation may form a reactive metabolite and bring some undesirable effects to human beings, such as idiosyncratic toxicity or mechanism-based inactivation of P450s (Kalgutkar and Dalvie, 2015). Inactivation of human P450s may result in clinically relevant herb-drug interactions (HDIs)/drug-drug interactions, particularly for those herbs or drugs containing time-dependent inactivators of P450s. Currently, the inhibition/inactivation potency of MOA on human P450s and related molecular mechanisms have not been reported. Thus, it is crucial to assay the potential inhibition and inactivation potentials of MOA against human P450s and to decipher the inhibitory mechanism of this homoisoflavonoid.

The major purposes of this study were to investigate reversible and time-dependent inhibition of human P450s by MOA and to decipher the molecular mechanisms for P450 inhibition or inactivation by MOA. For these purposes, the inhibition and inactivation potentials of MOA against human P450s were measured via performing a series of P450 inhibition assays. Meanwhile, the reactive metabolite(s) of MOA, and the key enzymes responsible for bioactivation of MOA, were identified by a panel of state-of-the-art techniques. The findings presented here provide key information for deep understanding of the interactions between MOA and human P450s, which would be very useful for the clinical applications of MOA and MOA-containing herbal products.

Materials and Methods

Chemicals, Reagents, and Biologic Samples. MOA (Fig. 1) and 5,7-dihydroxycoumarin were provided by Heowns Biochem Technologies (Tianjin, China). Chlorzoxazone, D-glucose-6-phosphate (G-6-P), testosterone, ketoconazole, glucose-6-phosphatedehydrogenase (G-6-PDH), propranolol, glutathione (GSH), β-NADP$^+$, and NADPH were all supplied by Sigma-Aldrich (St. Louis, MI). Phenacetin, $MgCl_2$, coumarin, omeprazole, paclitaxel, dextromethorphan, acetaminophen, potassium ferricyanide [$K_3Fe(CN)_6$], superoxide dismutase (SOD), and catalase (CAT) were ordered from Dalian Meilun Biotech (Dalian, China). The source of diclofenac was from Ark Pharm (Wuhan, China). 5-Hydroxyomeprazole and 6β-hydroxytestosterone were offered by TLC Pharmaceutical Standards (South Aurora, Canada). 6-Hydroxychlorzoxazone and 6α-hydroxytaxol were obtained from Torabto Research Chemicals (ON, Canada), and 4′-hydroxydiclofenac was ordered from Cayman Chemicals (Ann Arbor, Michigan). Lansoprazole was ordered from Hairong Pharmaceutical (Chengdu, China), and 7-hydroxycoumarin was supplied by Alfa Aesar (Heysham, UK). The purities of all compounds used in this study were greater than 98%. The recombinant human P450s and pooled human liver microsomes (HLMs, lot X008067) were all purchased from Bioreclamation IVT (Baltimore, MD). All biologic samples were stored at −80°C until use. The stock solution of each compound was dissolved in methanol and stored at 4°C until use. HPLC-grade acetonitrile and formic acid were acquired from Fisher (St. Louis, MI). Ultrapurified water, which was prepared by a Millipore purification system, was used throughout.

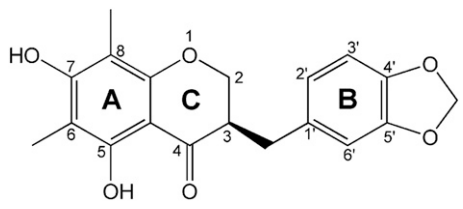

Fig. 1. The chemical structure of methylophiopogonanone A.

P450 Inhibition Assays. The procedure and in vitro incubation system (200 μl) for P450 inhibition assays were identical to the published literature (He et al., 2015; Wei et al., 2018; Fang et al., 2020), and the concentrations of the probe substrates as well as the incubation times for each P450 reaction are shown in Supplemental Materials. Briefly, the reaction was conducted in a mixed system containing PBS (100 mM, pH 7.4), NADPH regeneration system (1.0 mM β-NADP$^+$, 10 mM G-6-P, 1.0 U/ml G-6-PDH, and 4.0 mM $MgCl_2$), HLMs, and MOA. The reaction mixture was vortexed and prewarmed for 3 minutes at 37°C, and the oxidative reaction was started by adding each probe substrate. All incubation samples were incubated at 37°C for an additional 10–30 minutes (please see Supplemental Table 1 for details). The reactions were quenched by adding ice-cold acetonitrile (200 μl) containing internal standard lansoprazole or 5,7-dihydroxycoumarin [internal standard (IS)]. The mixtures were then centrifuged at 20,000*g* for 30 minutes at 4°C, the suspension liquid (100 μl) was diluted with Millipore water (100 μl), and then data were possessed by LC-MS/MS as depicted in Supplemental Table 2.

Time-dependent inhibition tests were conducted according to the previously reported procedure with slight modification (Obach et al., 2007; Fang et al., 2020). Briefly, a mixture containing PBS buffer, NADPH regeneration system (1.0 mM β-NADP$^+$, 10 mM G-6-P, 1.0 U/ml G-6-PDH, and 4.0 mM $MgCl_2$), HLMs, and MOA was vortexed for 10 seconds. After preliminary incubation at 37°C for 30 minutes, the reaction was subsequently initiated by addition of individual probe substrate. The reaction was performed at 37°C for an additional 10–30 minutes (the final concentrations of each P450 substrate and the incubation time are listed in Supplemental Table 1) before quenching the oxidative reaction. The supernatants were prepared in the same way as mentioned above and then analyzed by LC-MS/MS as shown in Supplemental Table 2.

Kinetic Analyses for Reversible Inhibition. To determine the types of inhibition and the values of K_i, MOA (0–10 μM) was incubated with HLMs supplemented with the NADPH-generating system, and each probe substrate was added in reaction mixture for 10–30 minutes at 37°C. The final concentrations of MOA and substrate for target P450 enzyme are shown in Supplemental Table 3. The residual activities of each enzymes were measured as described above. The kinetic data were then put into the equations below for competitive (a), noncompetitive (b), and mixed inhibition (c) mode, respectively.

a) $V = (V_{max}\mathrm{S})/[K_m(1 + \mathrm{I}/K_i) + \mathrm{S}]$;
b) $V = (V_{max}\mathrm{S})/\left[(K_m + \mathrm{S})(1 + \mathrm{I}/K_i)\right]$;
c) $V = (V_{max}\mathrm{S})/\left[(K_m + \mathrm{S})(1 + \mathrm{I}/\alpha K_i)\right]$.

Here, V represents the reaction velocity, V_{max} is the maximum reaction velocity, and S and I are the substrate and inhibitor (MOA) concentrations, respectively. K_m is the Michaelis constant of each P450 substrate,

and K_i is the inhibitory constant of MOA against a particular P450 enzyme.

Kinetic Analyses for Time-Dependent Inhibition. Inactivation kinetics of MOA against CYP2E1 and CYP2D6 were also performed by a dilution method, and the inhibition constant (K_I) and the maximum inactivation rate constant (k_{inact}) of MOA against CYP2E1-mediated chlorzoxazone hydroxylation and CYP2D6-mediated dextromethorphan *O*-demethylation were determined as follows. First, the incubation system (200 μl) containing PBS buffer, HLMs, G-6-P, G-6-PDH, $MgCl_2$, and MOA was vortexed, equilibrated, and then initiated by adding β-$NADP^+$. At 0, 5, 10, 20, or 30 minutes, respectively, 20 μl of aliquot was taken from the primary incubation mixture and then added to the secondary incubation mixture (total volume: 200 μl) containing PBS buffer, the NADPH regeneration system, and each probe substrate for a target P450. After incubation for another 20 minutes (CYP2E1) or 30 minutes (CYP2D6), the reaction was terminated by adding ice-cold acetonitrile (200 μl) containing lansoprazole or 5,7-dihydroxycoumarin (IS). Preparation of the samples for LC-MS/MS analysis was performed as mentioned above.

The inactivation kinetic parameters of both CYP2D6 and CYP2E1 by MOA were determined using the following equation:

$$K_{obs} = (k_{inact}I)/(K_I + I).$$

Here, [I] is the final concentration of MOA (inhibitor), k_{inact} represents the maximal rate constant of inactivation, and K_I means the inhibitor concentration required for 50% the maximal rate of inactivation.

Determination of NADPH-Dependent Inhibition of CYP2E1 by MOA. To determine the NADPH dependence of CYP2E1 inactivation, the samples were divided into three groups (A, B, and C). Group A was the mixture of PBS buffer, HLMs (1.0 mg/ml), and NADPH-generating system (as mentioned above), whereas group B was MOA (10 μM) mixed with PBS buffer, HLMs (1.0 mg/ml), and

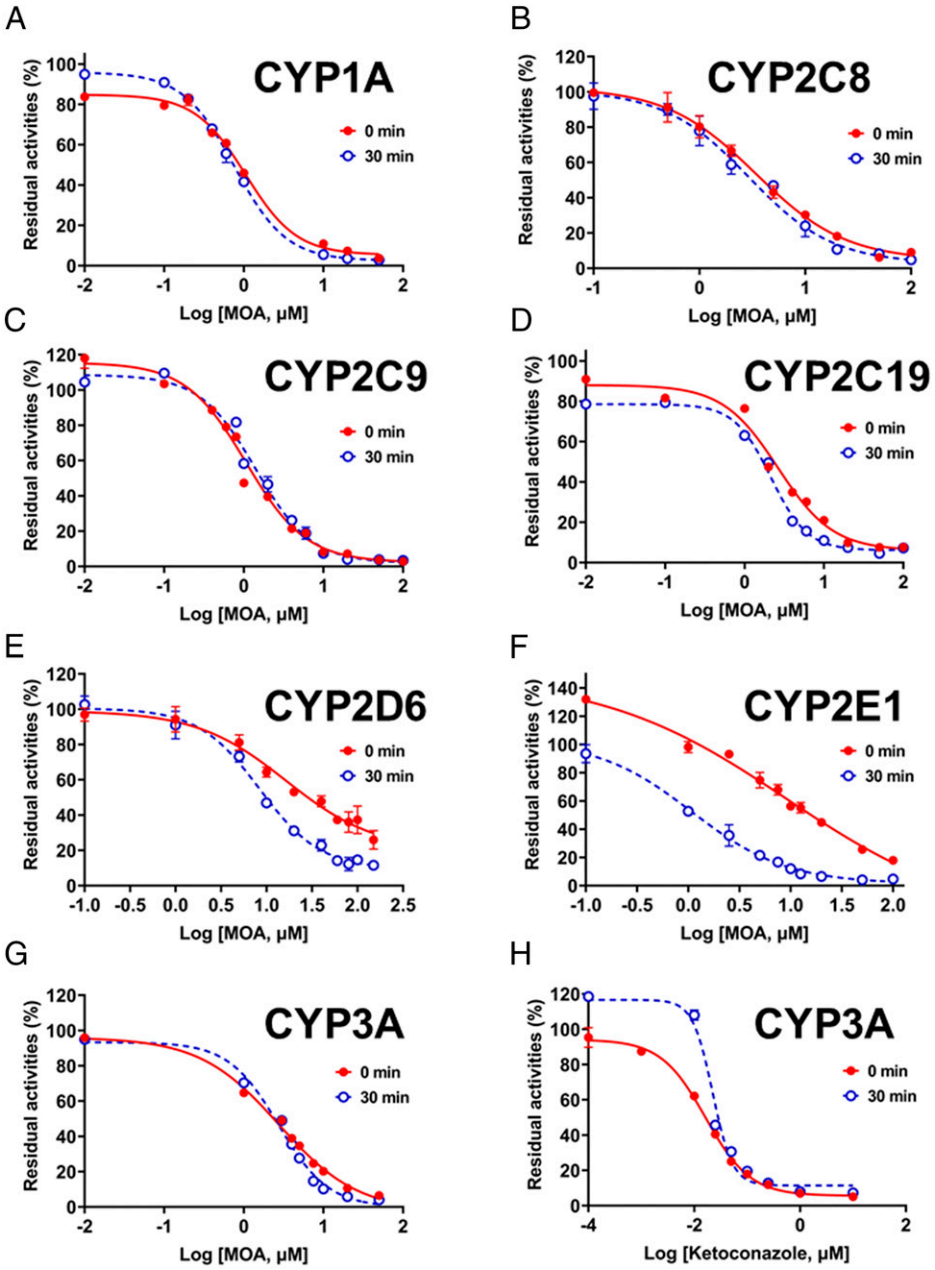

Fig. 2. The concentration-inhibition curves of MOA against CYP1A (A), CYP2C8 (B), CYP2C9 (C), CYP2C19 (D), CYP2D6 (E), CYP2E1 (F), and CYP3A (G) in HLMs with a 0- or 30-minute preincubation. The concentration-inhibition curve of ketoconazole against CYP3A in HLMs (H) with a 0- or 30-minute preincubation.

NADPH-generating system (as mentioned above). Group C contained MOA (10 μM) in PBS buffer (pH 7.4) containing G-6-P (10 mM), G-6-PDH (1.0 U/ml), and $MgCl_2$ (4.0 mM) but without β-$NADP^+$. At the time points of 0, 5, 10, 20, or 30 minutes, respectively, 20 μl of the aliquot was taken from the primary incubation mixture and then transferred to the secondary incubation mixture (total volume: 200 μl) that contained PBS, the NADPH-generating system, and chlorzoxazone. After a 20-minute incubation, refrigerated ice-cold acetonitrile (200 μl) containing 5,7-dihydroxycoumarin (IS) was added to completely end the reaction. The samples were prepared and analyzed as described above.

Determination Reversibility of MOA-Mediated CYP2E1 Inactivation. To investigate the mechanism of MOA-mediated CYP2E1 inactivation, the reversibility of MOA-mediated CYP2E1 inhibition was determined via testing the changes in residual activities with or without treatment of potassium ferricyanide [$K_3Fe(CN)_6$], as reported previously (Watanabe et al., 2007). First, the primary mixtures were incubated with HLMs (1.0 mg/ml), MOA (0 or 100 μM), and the NADPH-generating system in PBS buffer (pH 7.4). At the time intervals of 0, 5, 10, 20, or 30 minutes, 20 μl of the aliquot was transferred into the secondary solutions (20 μl) containing 100 mM PBS buffer with or without potassium ferricyanide (2.0 mM, final concentration). After incubating for another 10 minutes, the secondary incubation was diluted 5-fold with the final incubation solutions that contained PBS, the NADPH-generating system, and chlorzoxazone. The final incubation was continued for an additional 20 minutes before quenching the oxidation reaction by adding ice-cold acetonitrile (200 μl) containing 5,7-dihydroxycoumarin (IS).

The Effects of SOD/CAT and GSH on CYP2E1 Inactivation by MOA. The primary mixtures contained MOA (100 μM), HLMs, the NADPH-generating system and PBS in the presence of a mixture of SOD/CAT (800 U for each), GSH, or vehicle. After a 30-minute incubation under physiologically relevant conditions (pH 7.4, 37°C), 20 μl of aliquot was transferred into the secondary incubation mixture (total volume: 200 μl) that contained PBS, the NADPH-generating system, and chlorzoxazone. After another 20-minute incubation, the reactions were terminated by adding ice-cold acetonitrile (200 μl) containing 5,7-dihydroxycoumarin (IS).

Trapping the *O*-Quinone Metabolite by LC-MS/MS. To identify the potential *O*-quinone metabolite of MOA, GSH was used as a trapping agent. In brief, the incubation mixture containing PBS buffer, MOA (100 μM), $MgCl_2$ (3.2 mM), GSH (10 mM), and HLMs (1.0 mg protein/ml) was vortexed for 10 seconds and then placed at 37°C for a 3-minute preincubation. The oxidative reaction was initiated via adding NADPH (1.0 mM). After a 30-minute incubation, the reaction was terminated by ice-cold acetonitrile (equal volume) and then vortexed and centrifuged. The supernatants (5.0 μl) obtained from this reaction were injected into another LC-MS/MS system and then analyzed (Shenyang Laboratory).

Determination of P450 Enzymes Involved in MOA Bioactivation. To assign the key enzymes responsible for MOA bioactivation, MOA together with individual human recombinant P450s (100 nM), including CYP1A2, 2A6, 2C8, 2C9, 2C19, 2D6, 2E1, and 3A4, was incubated. The incubation conditions and sample processing were identical with those for the characterization of metabolites as above. The enzyme with the most effective catalysis was normalized to 100%.

Docking Simulations. To gain insight into the binding of MOA to the active pockets of three key enzymes (CYP2D6, 1A2, and 2E1) responsible for MOA bioactivation, AutoDock Vina (version 1.1.2) utilizing the Lamarckian genetic algorithm was employed to molecular docking calculation (Trott and Olson, 2010). The crystal structures of CYP2D6 (PDB: 3TDA), CYP1A2 (PDB: 2HI4), and CYP2E1 (PDB: 3KOH) were downloaded from Protein Data Bank (http://www.rcsb.org/pdb), followed by inputting MOA generated in ChemOffice (version 14.0). Water molecules in crystal structures were eliminated, and hydrogen atoms were added to the protein. Subsequently, Kollman charges were assigned. The grid box was set to 70 × 70 × 70 $Å^3$, with the spacing of 0.375. Then, MOA was docked within the active site of each P450 three-dimensional structure. The optimal conformers obtained on the basis of taking binding energy into consideration were held for further analyses.

Prediction of Herb-Drug Interaction Risks Triggered by MOA. To forecast the risks of potential herb-drug interactions triggered by MOA, we assessed the changes of the area under the plasma concentration-time curve (AUC) in the presence or absence of MOA. The interaction risk resulting from reversible inhibition was predicted using eq. 1. The risk caused by time-dependent inhibition of CYP2E1 and CYP2D6 was predicted using eq. 2 (Fang et al., 2010).

$$AUC_{ratio} = \frac{1}{f_{hep} \cdot \left(\frac{1/E_h}{(1/E_h-1)\bullet(1+I/K_i)+1}\right) + (1-f_{hep})}; \quad (1)$$

$$AUC_{ratio} = \frac{1}{\frac{f_{m,\,CYP}}{\left(1+\left(\frac{kinact\cdot[I]invivo}{K_{I,u}\cdot K\,\mathrm{deg}}\right)\right)} + (1-f_{m,\,CYP})}; \quad (2)$$

$$K_{I,u} = K_I \times f_{u,m}; \quad (3)$$

$$f_{u,\,m} = \frac{1}{C_{mic} \times 10^{0.56\bullet \mathrm{LogP}-1.41} + 1}. \quad (4)$$

The two primary parameters of eq. 1 were the fraction of hepatic clearance of the drugs mediated by P450s (f_{hep}) and the hepatic extraction ratio (E_h), respectively. I reflects the predicted maximum

TABLE 1

Inhibition parameters of MOA toward eight major P450s in human liver microsomes

Target Enzyme	Enzyme Source	IC_{50}	K_i or K_I	K_{inact}	Inhibition Mode	Goodness of Fit (R^2)
			μM	min^{-1}		
CYP1A	HLMs	1.06	1.71	—[a]	Competitive	0.98
CYP2A6	HLMs	>100	—	—	—	—
CYP2C8	HLMs	3.43	1.64	—	Competitive	0.99
CYP2C9	HLMs	1.07	2.87	—	Competitive	0.98
CYP2C19	HLMs	2.63	5.78	—	Competitive	0.97
CYP2D6	HLMs	16.38	207	0.07	Irreversible	0.98
CYP2E1	HLMs	9.13	20.90	0.03	Irreversible	0.99
CYP3A	HLMs	2.75	4.31	—	Noncompetitive	0.97

[a]None.

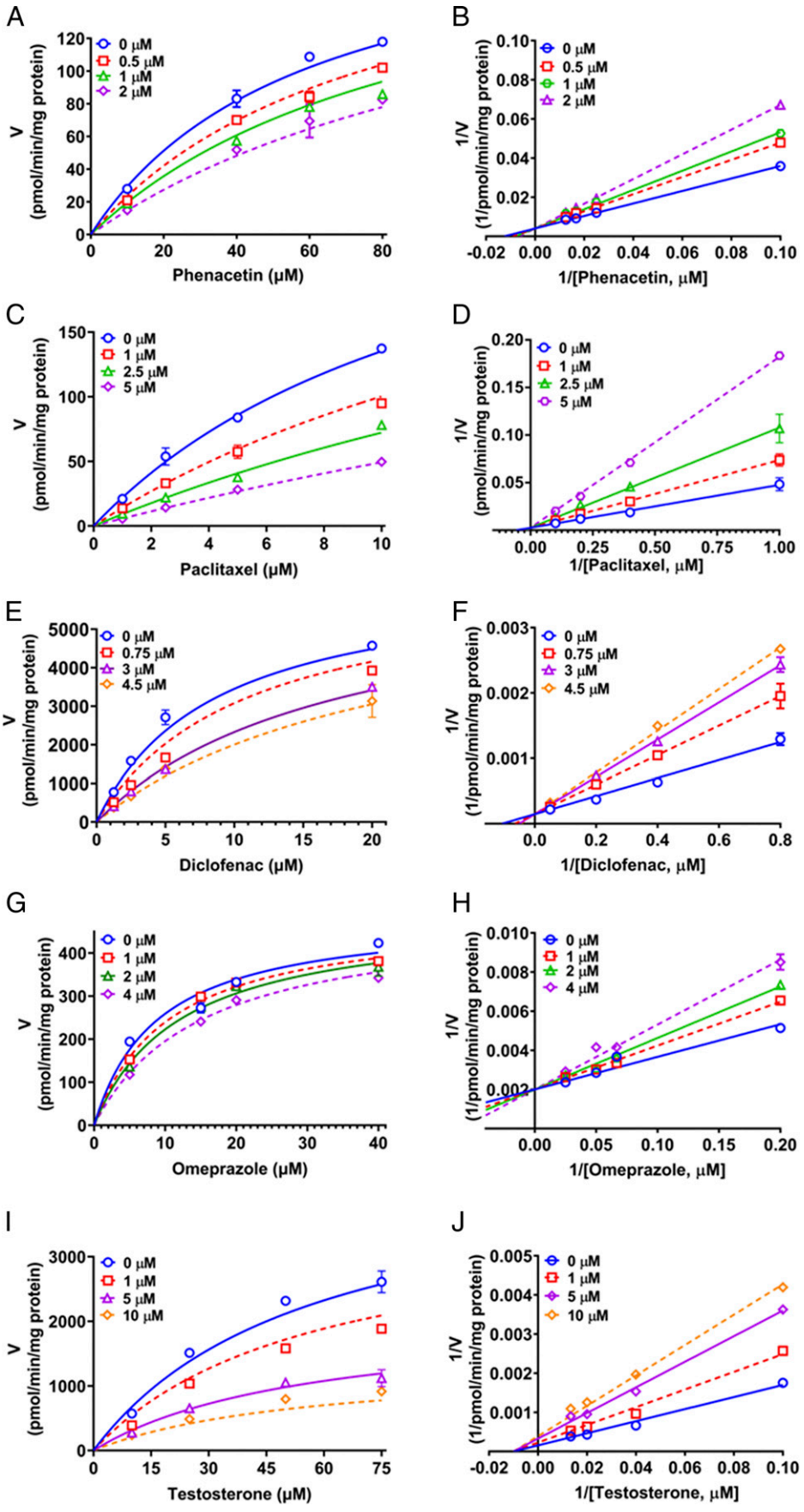

Fig. 3. Left: Lineweaver-Burk plots of MOA against CYP1A-mediated phenacetin *O*-deethylation (A), CYP2C8-mediated paclitaxel 6α-hydroxypaclitaxel (C), CYP2C9-mediated diclofenac 4′-hydroxylation (E), CYP2C19-mediated omeprazole 5-hydroxylation (G), and CYP3A-mediated testosterone 6β-hydroxylation (I) in HLM. Right: the corresponding second plots of the slopes from Lineweaver-Burk plots vs. MOA concentrations for CYP1A (B), 2C8 (D), 2C9 (F), 2C19 (H), and 3A (J), respectively.

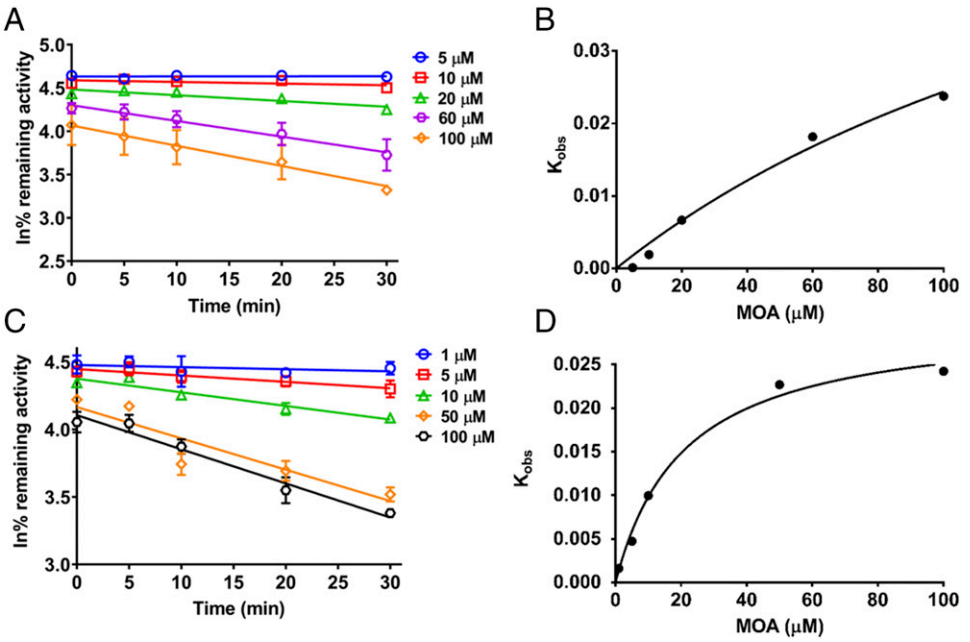

Fig. 4. Time-dependent inhibition of CYP2D6 and CYP2E1 by MOA. (A) Time- and dose-dependent inhibition of CYP2D6 by MOA. (B) The hyperbolic plot of k_{obs} of CYP2D6 vs. MOA concentrations. (C) Time- and dose-dependent inhibition of CYP2E1 by MOA. (D) The hyperbolic plot of k_{obs} of CYP2E1 vs. MOA concentrations.

concentration of MOA in human plasma, and K_i or K_I (micromolar) is the determined inhibitory constant of MOA against P450s. $K_{I,u}$ is the unbound K_I. The K_{deg} values of CYP2D6 and CYP2E1 are 0.000226 and 0.000192 minutes^{-1}, respectively (Obach et al., 2007). $f_{u,m}$ is free fraction of MOA in HLMs, and C_{mic} is microsomal protein concentration used in preincubation; C_{mic} for CYP2E1 was 1.0 mg/ml, and for CYP2D6 it was 2.0 mg/ml. ADMET laboratory was used to calculate the log P value of MOA as 2.87.

Data Analysis. The inhibition constants (including IC_{50} values, K_i, K_I, and k_{inact} values) were calculated by nonlinear regression, and all data are expressed as means ± S.D. of triplicate assays.

Results

Inhibitory Effects of MOA on Eight Human Hepatic P450s. To assess the inhibitory effects of MOA on eight key hepatic P450s, a preliminary assay was performed in HLMs fortified with MOA at final concentrations of 1.0, 10, and 100 μM. As shown in Supplemental Fig. 1, MOA displayed concentration-dependent inhibition on CYP1A, 2C9, 2C19, 3A, 2C8, 2E1, and 2D6 but not CYP2A6. After that, concentration-response curves of MOA on the formation rates of each oxidative metabolite in HLMs were plotted. As shown in Fig. 2, MOA concentration-dependently inhibited the catalytic activities of CYP1A, 2C8, 2C9, 2C19, 2D6, 2E1, and 3A, with IC_{50} values of 1.06, 3.43, 1.07, 2.63, 16.38, 9.13, and 2.75 μM, respectively (Table 1).

Time-Dependent Inhibition of MOA against Seven Human P450s. Next, time-course changes in the remaining P450 activities were determined in human microsomal incubations containing MOA and the NADPH-generating system. We found that a 30-minute preincubation of MOA with HLMs in the presence of NADPH could result in significant losses of CYP2D6 (from 16.38 to 8.35 μM of IC_{50}) and CYP2E1 (9.13 μM to 1.09 μM of IC_{50}) activities. By contrast, no such enzyme inhibitions were observed for CYP1A, 2C8, 2C9, 2C19, or 3A (the changes were less than 15%) (Fig. 2; Supplemental Table 4). These findings clearly demonstrated that MOA was a reversible inhibitor of CYP1A, 2C8, 2C9, 2C19, and 3A and that this agent was a time-dependent inhibitor of CYP2D6 and 2E1.

Inhibition Kinetics of MOA against Human P450s. Next, the inhibition kinetics of MOA against eight human hepatic P450s were investigated. As shown in Fig. 3, the Lineweaver-Burk plots clearly showed that MOA was a competitive inhibitor of CYP1A, CYP2C8, CYP2C9, and CYP2C19 in HLMs, whereas MOA acted as a noncompetitive inhibitor of CYP3A in HLMs. The K_i values for CYP1A, 2C8, 2C9, 2C19, and 3A were found to be 1.71, 1.64, 2.87, 5.78, and 4.31 μM, respectively.

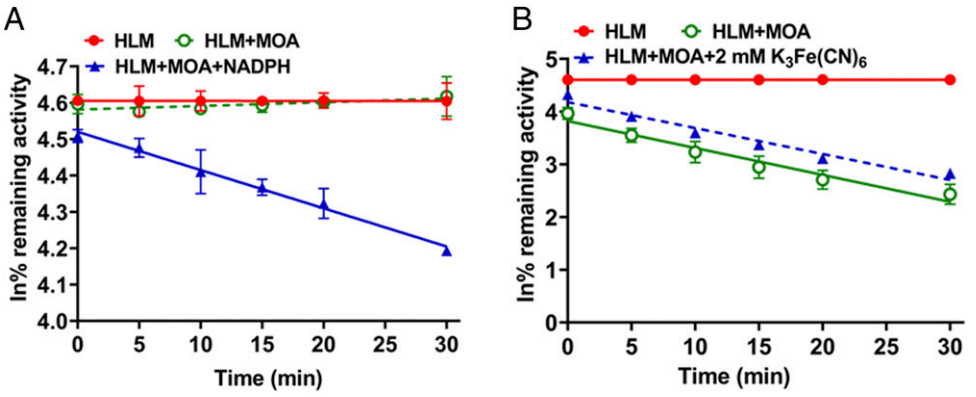

Fig. 5. (A) NADPH-dependent inhibition of CYP2E1 by MOA (10 μM). (B) The effects of $K_3Fe(CN)_6$ against CYP2E1 inactivation by MOA (100 μM).

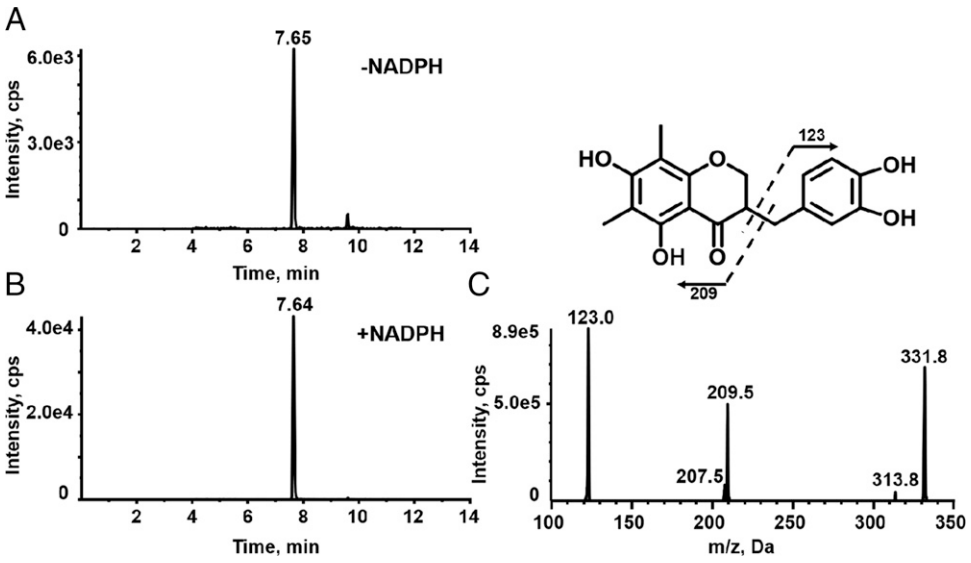

Fig. 6. Mass spectrometric characterization of the catechol metabolite. Extracted ion (*m/z* 331/123 for the catechol metabolite) chromatograms obtained from LC-MS/MS analysis of incubations containing HLMs and MOA with (A) or without (B) NADPH. (C) MS/MS spectrum of the catechol metabolite of MOA generated in microsomal incubations. cps, counts per second.

To assess the time-dependent inhibition of CYP2D6 and CYP2E1 by MOA, inactivation parameters K_I and k_{inact} values were determined in HLMs. As calculated from the plots of Fig. 4, the K_I, k_{inact}, and k_{inact}/K_I values of MOA for CYP2D6 were found to be 207 μM, 0.07 minutes^{-1}, and 3.38 × 10^{-4} minutes^{-1}μM^{-1}, respectively, whereas the K_I, k_{inact}, and k_{inact}/K_I values for CYP2E1 were 20.9 μM, 0.03 minutes^{-1}, and 14.4 × 10^{-4} minutes^{-1}μM^{-1}, respectively. Clearly, MOA inactivated CYP2E1 more potently than CYP2D6.

NADPH-Dependent Inhibition of CYP2E1 by MOA. Next, NADPH-dependent inhibition assay was conducted to determine whether the time-dependent inhibition of MOA against CYP2E1 was NADPH-dependent. As shown in Fig. 5A, coincubation with CYP2E1 and MOA (10 μM) without NADPH did not decrease the catalytic activity of CYP2E1. In sharp contrast, a 30-minute coincubation of HLMs with MOA (10 μM) in the NADPH-generating system resulted in significant loss of CYP2E1 activity (35%). These findings clearly suggested that the observed CYP2E1 inhibition was NADPH-dependent and that such a process required the metabolic activation by the host P450 enzyme(s).

Effects of Potassium Ferricyanide on MOA-Mediated CYP2E1 Inactivation. Potential involvement of carbene in the P450 inactivation was probed by coincubation with potassium ferricyanide (Watanabe et al., 2007), which would reverse the inhibition that resulted from carbene-Fe^{2+} chelation (Fig. 10) by oxidation of ferrous ion of the host enzyme. Herein, we investigated the effects of potassium ferricyanide on MOA-mediated CYP2E1 inactivation. As shown in Fig. 5B, potassium ferricyanide failed to show the protective effect against the inactivation of CYP2E1 (less than 20%) induced by MOA. This finding suggested that carbene intermediate (Fig. 10A) did not participate in the inactivation of CYP2E1.

Identification of *O*-Quinone Metabolite of MOA. Next, the reactive metabolite(s) of MOA in HLMs in the NADPH-generating system was trapped by GSH. As shown in Fig. 6, a single product peak (retention time = 7.64 minutes) with a pseudomolecular ion $[M + H]^+$ at *m/z* 331 (12 Da less than that of the parent drug) was observed from the incubation mixture, indicating that MOA experienced a loss of carbon during oxidation by microsomal proteins. The mass spectrum of the product revealed product ions *m/z* 123 and *m/z* 209, suggesting that an *O*-demethylenation took place to form the corresponding catechol metabolite (Fig. 10B). Additionally, we succeeded in detection of a GSH conjugate–derived ($[M + H]^+$ at *m/z* = 636, retention time = 5.84 minutes, Fig. 7) *O*-quinone intermediate (Fig. 10D). The product ion of MOA-GSH conjugate possessed a characteristic loss of GSH moiety,

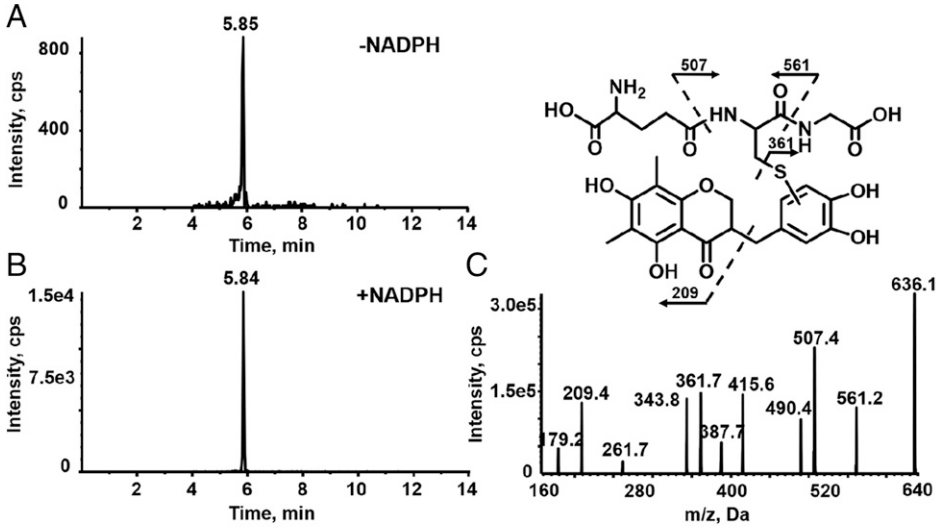

Fig. 7. Mass spectrometric characterization of the GSH-adduct after incubation of MOA in HLMs in NADPH-generating system. Extracted ion (*m/z* 636/507 for GSH-adduct) chromatograms obtained from LC-MS/MS analysis of incubations containing HLM, MOA, and GSH in the absence (A) or presence (B) of NADPH. (C) MS/MS spectrum of GSH-adduct generated in microsomal incubations.

TABLE 2

Effects of GSH and SOD/catalase on the inactivation of CYP2E1 by MOA (100 μM)

Agents	Remaining Activities
	%
MOA	18.85 ± 0.51
MOA + GSH	15.60 ± 0.35
MOA + SOD + CAT	17.70 ± 0.91

including 75 Da ($C_2H_5O_2N$, loss of glycinyl moiety), 129 Da ($C_5H_7O_3N$, neutral loss of γ-glutamyl moiety), and 275 Da ($C_{10}H_{16}O_6N_3$, cleavage of C-S bond moiety of GSH). Both the catechol metabolite and MOA-GSH-adduct shared the same product ion at *m/z* 209, revealing that the A-C ring system retained intact. By contrast, trace amount of MOA-GSH conjugate was found in the negative incubations without addition of NADPH (Fig. 7A). The detection of MOA-GSH conjugate suggests that quinone metabolite (Fig. 10D) could be formed and that this reactive intermediate might inactivate the host P450 enzymes via modification of the cystines in the host enzyme.

Effects of SOD/Catalase and GSH on MOA-Mediated CYP2E1 Inactivation. Subsequently, the effects of GSH and SOD/CAT on MOA-mediated CYP2E1 inactivation were also investigated. As shown in Table 2, after a 30-minute incubation, the residual activities of CYP2E1 with GSH (15.6% ± 0.35%) were much closed to that without GSH (18.85% ± 0.51%). This finding suggested that GSH could not block CYP2E1 inactivation, implying that CYP2E1 inactivation possibly happened in the active site of CYP2E1. Additionally, the mixture of SOD and CAT, as reactive oxygen species scavenger, displayed weak effects on MOA-mediated CYP2E1 inactivation. This finding indicated that reactive oxygen species made limited contribution to the enzyme inactivation.

P450s Participating in MOA Bioactivation. To recognize the key P450 enzyme(s) responsible for the bioactivation of MOA, eight major hepatic human recombinant P450s were individually incubated with MOA in the presence of both GSH and NADPH, followed by quantification of the formation rates of the MOA-GSH conjugate. CYP2D6, 1A2, and 2E1 were found to be the major contributors to catalyze the metabolic activation of MOA to form a catechol metabolite that could be captured by GSH, whereas CYP3A4, 2A6, 2C8, 2C9, and 2C19 contributed to a lesser extent (Fig. 8). Clearly, multiple human hepatic P450s could catalyze the metabolic activation of MOA.

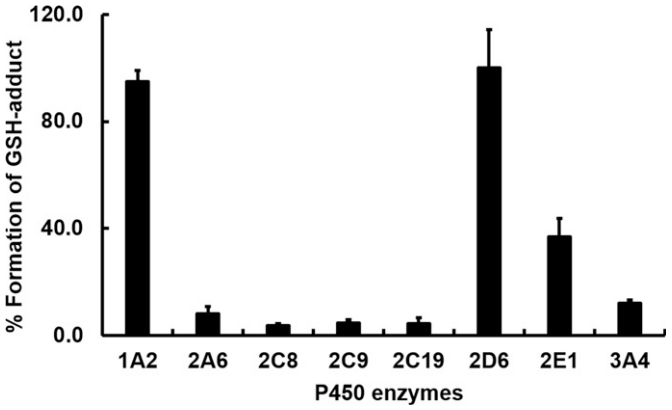

Fig. 8. The formation rates of GSH-adduct in incubations of MOA with individual recombinant P450 enzymes after normalization on the basis of the relative content of the corresponding P450 enzyme in human liver microsomes.

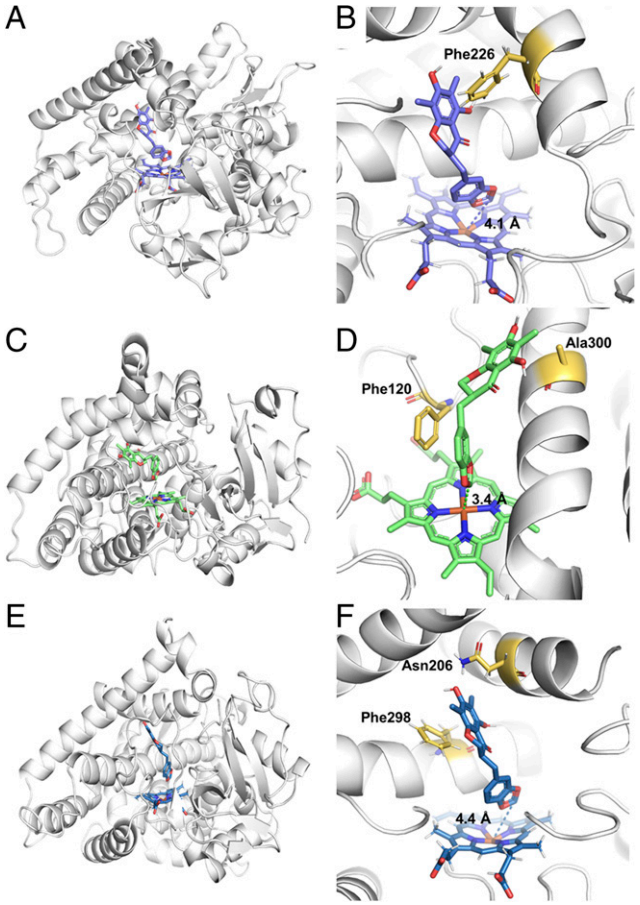

Fig. 9. The binding poses of MOA in the active pocket of CYP1A2, CYP2D6, or CYP2E1. (A) A stereo view of CYP1A2 docked with MOA. (B) A detailed view of MOA bound at the active pocket of CYP1A2. (C) A stereo view of CYP2D6 docked with MOA. (D) A detailed view of MOA bound at the active pocket of CYP2D6. (E) A stereo view of CYP2E1 docked with MOA. (F) A detailed view of MOA bound at the active pocket of CYP2E1.

Docking Simulations of MOA in CYP1A2, CYP2D6, and CYP2E1. To better decipher the interactions between MOA and CYP1A2, 2D6, and 2E1 at molecular levels, docking simulations of MOA into these three key hepatic P450s that catalyzed the bioactivation of this agent were carried out. As drawn in Figs. 9 and 10, MOA could be tightly docked into the catalytic cavity of CYP1A2, 2D6, and 2E1, whereas the carbon atom of MDP moiety in MOA was positioned toward the heme, with the distance between the carbon atom of MDP and the heme iron being 3.4, 4.1, and 4.4 Å in CYP2D6, 1A2, and 2E1, respectively. Meanwhile, the binding energies of the lowest-energy conformations of MOA in these three P450s were also predicted as −9.8, −9.3, and −8.8 kcal/mol for CYP2D6, 1A2, and 2E1, respectively (Supplemental Table 5). In addition, the key interactions between MOA and these three P450s were also investigated. As depicted in Supplemental Figs. 3–5, rings A and B of MOA could interact with some key residuals and heme in the catalytic cavity of CYP1A2, 2D6, and 2E1 mainly via hydrophobic interactions, such as π-π stacking and π-alkyl interactions. These findings suggested that MOA could enter into the catalytic cavities of CYP1A2, 2D6, and 2E1 and that these enzymes could activate this agent via oxidation of the carbon atom in the MDP moiety of MOA.

Quantitative Predictions of the HDI Risks Triggered by MOA. Finally, the risks of HDIs triggered by MOA were predicted by using a set of in vitro inhibition data. The magnitudes of the potential HDI between P450 substrate drugs and MOA-related products were

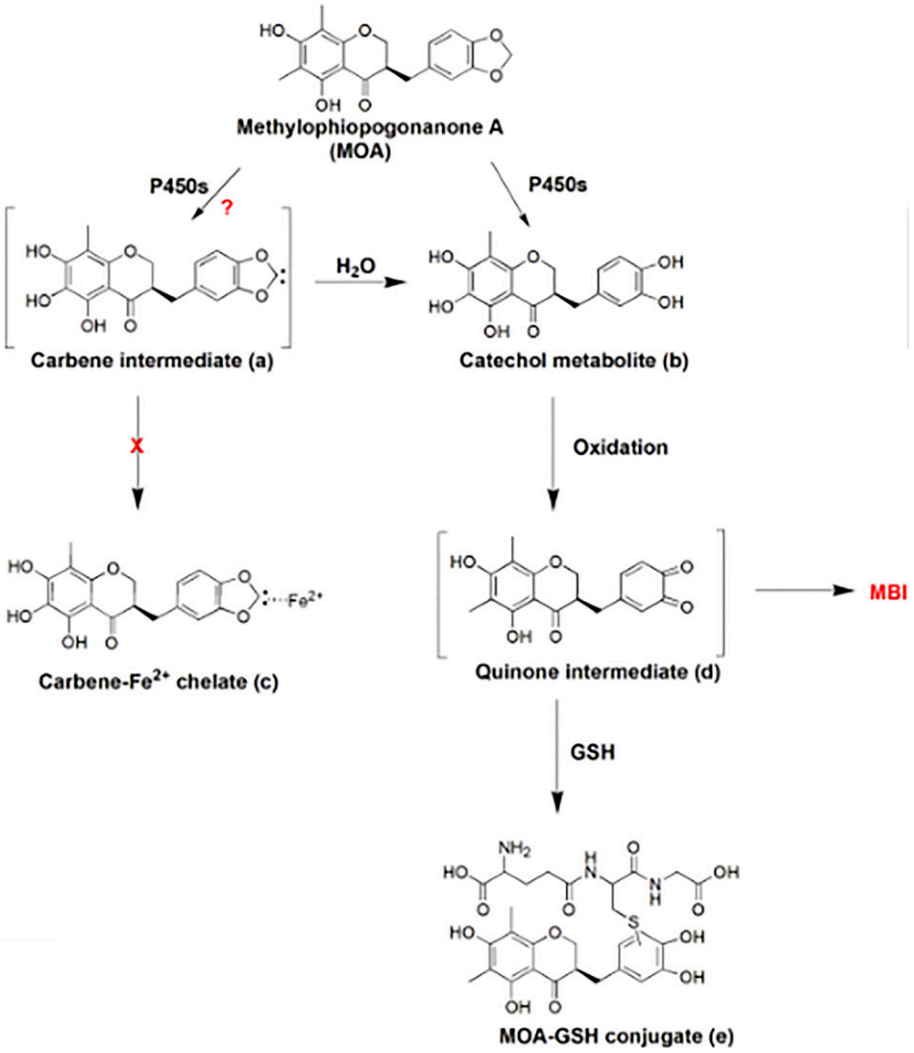

Fig. 10. Proposed pathways for the formation of reactive intermediate and MOA-GSH conjugate by P450-mediated bioactivation of MOA.

estimated by increase of AUC in the presence of the MOA. As shown in Table 3, MOA hardly triggered a significant increase in AUC of the substrate drugs that were predominately metabolized by human hepatic CYP1A2, 2C8, 2C9, 2C19, and 3A4. By contrast, MOA, the irreversible inactivator of CYP2D6 and CYP2E1, could trigger dramatic increase in the AUC of the substrate drugs that were predominately metabolized by human CYP2D6 and CYP2E1, especially the substrate drugs of CYP2E1. These findings suggested that MOA-related herbal

TABLE 3

Prediction of the potential HDI risks of MOA via inhibition on human hepatic P450s

Target P450	E_h[a]	F_{hep} (or $f_{m,CYP}$)[b]	I[c]	AUC Ratios[d]	AUC Increased
			μM		%
CYP1A	0.1–0.9	0.8	0.05–0.25	1.00–1.10	0–10
CYP2C8				1.00–1.11	0–11
CYP2C9				1.00–1.06	0–6
CYP2C19				1.00–1.03	0–3
CYP3A				1.00–1.04	0–4
CYP2D6				1.23–1.94	23–94
CYP2E1				1.64–2.96	64–196

[a]The hepatic extraction ratio (E_h) was set between 0.1 and 0.9.
[b]For reversible inhibition, the f_{hep} was set to the mean value of each P450 substrates. For irreversible inhibition, the $f_{m,\ CYP2D6}$ and $f_{m,\ CYP2E1}$ was set to 0.8 in CYP2D6 or CYP2E1 isoforms.
[c]I was the C_{max} value of MOA in human plasma. MOA accounts for approximately 0.004%–0.019% (w/w) of *Ophiopogon*, whereas the *Chinese Pharmacopoeia* (version 2015) recommended the daily dosage of *Ophiopogon* as up to 12 g. The oral bioavailability of MOA was predicted as 20% by using ADMETlab (http://admet.scbdd.com/calcpre/calc_cf_single_mol), and the volume of blood in adults is approximately 5.2 l. On the basis of the abovementioned data, the C_{max} value of MOA in human plasma was calculated as 0.05–0.25 μM.
[d]The methods for prediction of the changes in AUC were described in *Prediction of Herb-Drug Interaction Risks Triggered by MOA*.

medicines might trigger HDI when MOA-related products were coadministered with CYP2D6 and CYP2E1 substrate drugs.

Discussion

In view of the fact that *O. radix*–related herbal products are commonly used in combination with some synthetic pharmaceutical agents for treating angiocardiopathy and different types of cancer (Chen et al., 2016a; Liu et al., 2017; Duan et al., 2018; Fan et al., 2020), the potential risks of the HDIs should be carefully examined. Although the molecular mechanisms of HDIs are diverse, most cases of the clinically relevant HDIs are related with pharmacokinetic alterations (Qin et al., 2017; Sun et al., 2017; Dunkoksung et al., 2019; Ge, 2019) in which coadministered herbal products alter the function or expression of drug-metabolizing enzymes or transporters that are responsible for the elimination of the therapeutic agents. Unfortunately, to date, the interactions between the major constituents in *O. radix* and drug-metabolizing enzymes in humans are rarely investigated.

In this study, MOA, one of the most abundant constituents in the Chinese herb mai-dong, was selected as a representative compound of naturally occurring homoisoflavonoids to assay its inhibitory effects against human P450s and to decipher the inhibitory mechanism of this homoisoflavonoid. The results obtained from this work clearly demonstrated that MOA was a reversible inhibitor of CYP1A, 2C8, 2C9, 2C19, and 3A but that this agent acted as an irreversible inhibitor of CYP2D6 and CYP2E1. In these cases, the potential risks of MOA to trigger HDI via P450 inhibition or inactivation were routinely predicted by using in vitro inhibition constants and their pharmacokinetic parameters. As shown in Table 3, MOA hardly triggered significant increases in the AUC of the substrate drugs that were predominately metabolized by human hepatic CYP1A, 2C8, 2C9, 2C19, and 3A. By contrast, MOA may result in an obvious increase in the AUC of the substrate drugs that were predominately metabolized by human CYP2D6 and CYP2E1. Considering that the MOA-related herbal products are always used long-term in some aged patients, enhanced attention should be paid on the potential risks of herb-drug interactions between MOA-related products and CYP2D6/CYP2E1 substrate drugs. It also should be noted that most of CYP2E1 substrate drugs (such as chlorzoxazone) have relatively wide therapeutic windows and that these agents are rarely used in combination with *O. radix*–related products; it is unlikely to trigger clinically relevant HDIs when *O. radix*–related products are coadministered with CYP2E1 substrate drugs. For CYP2D6, it is well known that this enzyme participates in the metabolic clearance of over 25% of therapeutic agents (Carrão et al., 2019), such as antiarrhythmics (encainide, etc.), antihypertensives (nicergoline, etc.), and antidepressants (clomipramine, etc.). In these cases, the combination use of MOA-related products with the drugs prominently metabolized by CYP2D6 should be used with caution to avoid the occurrence of clinically relevant HDIs, especially those CYP2D6-substrate drugs possessing narrow therapeutic index (such as dextromethorphan, metoprolol, and venlafaxine) (Zhou, 2009).

It should also be noted that inhibition or dysfunction of human P450s is a double-edged sword and, in some cases, may result in beneficial effects for human health. For example, inactivation of CYP2E1 and CYP2D6 could block the metabolic activation of some drugs or toxins, such as acetaminophen, isoniazid, tamoxifen, and styrene (Fan and Bolton, 2001; Chen et al., 2019). Inactivation of CYP2E1 and CYP2D6 by MOA may block the formation of the reactive metabolites of these agents in part, which in turn reduces the adduct of biomolecules, such as protein and DNA, derived from these reactive metabolites (Fan and Bolton, 2001; Zembutsu et al., 2011; Chen et al., 2019). Therefore, it is easily conceivable that MOA may be beneficial for alleviating the idiosyncratic toxicity or hepatoxicity of acetaminophen, isoniazid tamoxifen, and styrene by considering that these agents could be activated by CYP2E1 or CYP2D6.

Furthermore, both CYP1A and CYP2E1 have been validated as the crucial enzymes responsible for the activation of some known procarcinogens (such as benzopyrene, nitrate, and aflatoxin) to their carcinogenic metabolites (Zhou et al., 2009; Chen et al., 2019); thus, these two P450s have been considered as key targets for preventing various types of cancer. Meanwhile, CYP2E1 also plays a crucial role in oxidation of ethanol, which converted ethanol to acetate in the human body and might result in immunogenic reactions and alcoholic liver injury (Chen et al., 2019). Increasing evidence has demonstrated that CYP1A or CYP2E1 inhibitor therapy may partially block CYP1A- or CYP2E1-mediated activation of procarcinogens and ethanol, which in turn reduces the risks of certain cancers and alcoholic hepatotoxicity. In the present study, our findings clearly demonstrate that MOA strongly inhibits CYP1A (IC_{50} = 1.06 μM, K_i = 1.71 μM) and potently inactivates CYP2E1 (K_I = 20.9 μM; k_{inact} = 0.03 minutes^{-1}), which partially explains the cancer-preventive effects of MOA and suggests that MOA is a drug with great promise for the development of dual inhibitors against both CYP1A and CYP2E1. As one of the most abundant constituents in *O. radix*, MOA could be isolated from this herb, and its chemical structure could be easily modified by the chemists to generate a series of MOA derivatives. Therefore, in the future, a series of MOA derivatives should be obtained to study the structure-P450 inhibition activity relationships, which will be very useful for designing and developing novel cancer-preventive agents via targeting procarcinogen-activating P450s.

Authorship Contributions

Participated in research design: Zheng, Ge.

Conducted experiments: Tu, Mao.

Contributed new reagents or analytic tools: Zhang, He, J.-J. Wu, Zhao.

Performed data analysis: Tu, Mao.

Wrote or contributed to the writing of the manuscript: Tu, Mao, Y. Wu, Zheng, Ge.

References

Carrão DB, Habenchus MD, de Albuquerque NCP, da Silva RM, Lopes NP, and de Oliveira ARM (2019) In vitro inhibition of human CYP2D6 by the chiral pesticide fipronil and its metabolite fipronil sulfone: prediction of pesticide-drug interactions. *Toxicozl Lett* **313**:196–204.

Chen L, Liu L, Chen Y, Liu M, Xiong Y, Zhang H, Huang S, and Xia C (2019) Modulation of transporter activity of OATP1B1 and OATP1B3 by the major active components of Radix Ophiopogonis. *Xenobiotica* **49**:1221–1228.

Chen MH, Chen XJ, Wang M, Lin LG, and Wang YT (2016a) Ophiopogon japonicus–A phytochemical, ethnomedicinal and pharmacological review. *J Ethnopharmacol* **181**:193–213.

Chen X, Zhao Z, Chen Y, Gou X, Zhou Z, Zhong G, Cai Y, Huang M, and Jin J (2016b) Mechanistic understanding of the effect of Dengzhan Shengmai capsule on the pharmacokinetics of clopidogrel in rats. *J Ethnopharmacol* **192**:362–369.

Duan B, Xie J, Rui Q, Zhang W, and Xi Z (2018) Effects of Shengmai injection add-on therapy to chemotherapy in patients with non-small cell lung cancer: a meta-analysis. *Support Care Cancer* **26**:2103–2111.

Dunkoksung W, Vardhanabhuti N, Siripong P, and Jianmongkol S (2019) Rhinacanthin-C mediated herb-drug interactions with drug transporters and phase I drug-metabolizing enzymes. *Drug Metab Dispos* **47**:1040–1049.

Fan H, Liu S, Shen W, Kang A, Tan J, Li L, Liu X, Xu C, Xu X, Lai Y, et al. (2020) Identification of the absorbed components and metabolites of Xiao-Ai-Jie-Du decoction and their distribution in rats using ultra high-performance liquid chromatography/quadrupole time-of-flight mass spectrometry. *J Pharm Biomed Anal* **179**:112984.

Fan PW and Bolton JL (2001) Bioactivation of tamoxifen to metabolite E quinone methide: reaction with glutathione and DNA. *Drug Metab Dispos* **29**:891–896.

Fang J, Wang X, Lu M, He X, and Yang X (2018) Recent advances in polysaccharides from Ophiopogon japonicus and Liriope spicata var. prolifera. *Int J Biol Macromol* **114**:1257–1266.

Fang SQ, Huang J, Zhang F, Ni HM, Chen QL, Zhu JR, Fu ZC, Zhu L, Hao WW, and Ge GB (2020) Pharmacokinetic interaction between a Chinese herbal formula Huosu Yangwei oral liquid and apatinib in vitro and in vivo. *J Pharm Pharmacol* **72**:979–989.

Fang ZZ, Zhang YY, Ge GB, Huo H, Liang SC, and Yang L (2010) Time-dependent inhibition (TDI) of CYP3A4 and CYP2C9 by noscapine potentially explains clinical noscapine-warfarin interaction. *Br J Clin Pharmacol* **69**:193–199.

Ge GB (2019) Deciphering the metabolic fates of herbal constituents and the interactions of herbs with human metabolic system. *Chin J Nat Med* **17**:801–802.

He F, Xu BL, Chen C, Jia HJ, Wu JX, Wang XC, Sheng JL, Huang L, and Cheng J (2016) Methylophiopogonanone A suppresses ischemia/reperfusion-induced myocardial apoptosis in mice via activating PI3K/Akt/eNOS signaling pathway. *Acta Pharmacol Sin* **37**:763–771.

He W, Wu JJ, Ning J, Hou J, Xin H, He YQ, Ge GB, and Xu W (2015) Inhibition of human cytochrome P450 enzymes by licochalcone A, a naturally occurring constituent of licorice. *Toxicol In Vitro* **29**:1569–1576.

Kalgutkar AS and Dalvie D (2015) Predicting toxicities of reactive metabolite-positive drug candidates. *Annu Rev Pharmacol Toxicol* **55**:35–54.

Li N, Zhang JY, Zeng KW, Zhang L, Che YY, and Tu PF (2012) Anti-inflammatory homoisoflavonoids from the tuberous roots of Ophiopogon japonicus. *Fitoterapia* **83**:1042–1045.

Liang H, Xing Y, Chen J, Zhang D, Guo S, and Wang C (2012) Antimicrobial activities of endophytic fungi isolated from Ophiopogon japonicus (Liliaceae). *BMC Complement Altern Med* **12**: 238.

Lin Y, Zhu D, Qi J, Qin M, and Yu B (2010) Characterization of homoisoflavonoids in different cultivation regions of Ophiopogon japonicus and related antioxidant activity. *J Pharm Biomed Anal* **52**:757–762.

Liu WY, Zhang JW, Yao XQ, Jiang C, He JC, Ni P, Liu JL, Chen QY, Li QR, Zang XJ, et al. (2017) Shenmai injection enhances the cytotoxicity of chemotherapeutic drugs against colorectal cancers via improving their subcellular distribution. *Acta Pharmacol Sin* **38**:264–276.

Ma C, Li G, Zhang J, Zheng Q, Fan X, and Wang Z (2009) An efficient combination of supercritical fluid extraction and high-speed counter-current chromatography to extract and purify homoisoflavonoids from Ophiopogon japonicus (Thunb.) Ker-Gawler. *J Sep Sci* **32**:1949–1956.

Obach RS, Walsky RL, and Venkatakrishnan K (2007) Mechanism-based inactivation of human cytochrome p450 enzymes and the prediction of drug-drug interactions. *Drug Metab Dispos* **35**: 246–255.

Qin X, Lu J, Wang P, Xu P, Liu M, and Wang X (2017) Cytochrome P450 3A selectively affects the pharmacokinetic interaction between erlotinib and docetaxel in rats. *Biochem Pharmacol* **143**:129–139.

Sun J, Lu Y, Li Y, Pan J, Liu C, Gong Z, Huang J, Zheng J, Zheng L, Li Y, et al. (2017) Influence of shenxiong glucose injection on the activities of six CYP isozymes and metabolism of warfarin in rats assessed using probe cocktail and pharmacokinetic approaches. *Molecules* **22**:1994.

Tan M, Chen J, Wang C, Zou L, Chen S, Shi J, Mei Y, Wei L, and Liu X (2019) Quality evaluation of ophiopogonis radix from two different producing areas. *Molecules* **24**:3220.

Tian Y, Gong P, Wu Y, Chang S, Xu J, Yu B, and Qi J (2019) Screening and identification of potential active components in Ophiopogonis Radix against atherosclerosis by biospecific cell extraction. *J Chromatogr B Analyt Technol Biomed Life Sci* **1133**:121817.

Trott O and Olson AJ (2010) AutoDock Vina: improving the speed and accuracy of docking with a new scoring function, efficient optimization, and multithreading. *J Comput Chem* **31**:455–461.

Wang J, Liu HQ, Liu L, Tang HT, Zhang P, and Tang Y (2013) [Development of full-quantified HPLC fingerprint for quality evaluation of ophiopogonis radix of sichuan]. *Zhong Yao Cai* **36**: 721–725.

Wang L, Zhou Y, Qin Y, Wang Y, Liu B, Fang R, and Bai M (2019) Methylophiopogonanone B of Radix Ophiopogonis protects cells from H2O2-induced apoptosis through the NADPH oxidase pathway in HUVECs. *Mol Med Rep* **20**:3691–3700.

Wang Y, Liu F, Liang Z, Peng L, Wang B, Yu J, Su Y, and Ma C (2017) Homoisoflavonoids and the antioxidant activity of *Ophiopogon japonicus* root. *Iran J Pharm Res* **16**:357–365.

Watanabe A, Nakamura K, Okudaira N, Okazaki O, and Sudo K (2007) Risk assessment for drug-drug interaction caused by metabolism-based inhibition of CYP3A using automated in vitro assay systems and its application in the early drug discovery process. *Drug Metab Dispos* **35**: 1232–1238.

Wei J, Zhang H, and Zhao Q (2018) In vitro inhibitory effects of Friedelin on human liver cytochrome P450 enzymes. *Pharm Biol* **56**:363–367.

Xia CH, Sun JG, Wang GJ, Shang LL, Zhang XX, Zhang R, Peng Y, Wang XJ, Hao HP, Xie L, et al. (2010) Herb-drug interactions: in vivo and in vitro effect of Shenmai injection, a herbal preparation, on the metabolic activities of hepatic cytochrome P450 3A1/2, 2C6, 1A2, and 2E1 in rats. *Planta Med* **76**:245–250.

Zembutsu H, Sasa M, Kiyotani K, Mushiroda T, and Nakamura Y (2011) Should CYP2D6 inhibitors be administered in conjunction with tamoxifen? *Expert Rev Anticancer Ther* **11**:185–193.

Zhan T, Yao N, Wu L, Lu Y, Liu M, Liu F, Xiong Y, and Xia C (2019) The major effective components in Shengmai Formula interact with sodium taurocholate co-transporting polypeptide. *Phytomedicine* **59**:152916.

Zhao M, Xu WF, Shen HY, Shen PQ, Zhang J, Wang DD, Xu H, Wang H, Yan TT, Wang L, et al. (2017) Comparison of bioactive components and pharmacological activities of ophiopogon japonicas extracts from different geographical origins. *J Pharm Biomed Anal* **138**:134–141.

Zhou SF (2009) Polymorphism of human cytochrome P450 2D6 and its clinical significance: Part I. *Clin Pharmacokinet* **48**:689–723.

Zhou SF, Chan E, Zhou ZW, Xue CC, Lai X, and Duan W (2009) Insights into the structure, function, and regulation of human cytochrome P450 1A2. *Curr Drug Metab* **10**:713–729.

Zhu YZ, Huang SH, Tan BK, Sun J, Whiteman M, and Zhu YC (2004) Antioxidants in Chinese herbal medicines: a biochemical perspective. *Nat Prod Rep* **21**:478–489.

Address correspondence to: Jiang Zheng, Wuya College of Innovation, Shenyang Pharmaceutical University, Wenhua Road 103, Shenyang 110016, China. E-mail: zhengneu@yahoo.com; or Guang-Bo Ge, Institute of Interdisciplinary Integrative Medicine Research, Shanghai University of Traditional Chinese Medicine, Shanghai 201203, China. E-mail: geguangbo@dicp.ac.cn